28. V. S. Malinin, M. E. Haque, B. R. Lentz, *Biochemistry* **40**, 8292 (2001).
29. L. D. Mayer, M. J. Hope, P. R. Cullis, *Biochim. Biophys. Acta* **858**, 61 (1986).
30. R. Nayer, M. J. Hope, P. R. Cullis, *Biochim. Biophys. Acta* **986**, 200 (1989).
31. S. G. Clerc, T. E. Thompson, *Biophys. J.* **67**, 475 (1994).
32. D. G. Hunter, B. J. Frisken, *Biophys. J.* **74**, 2996 (1998).
33. B. J. Frisken, C. Asman, P. J. Patty, *Langmuir* **16**, 928 (2000).
34. B. L.-S. Mui, H.-G. Döbereiner, T. D. Madden, P. R. Cullis, *Biophys. J.* **69**, 930 (1995).
35. M. Traïkia, D. E. Warschawski, O. Lambert, J.-L. Rigaud, P. F. Devaux, *Biophys. J.* **83**, 1443 (2002).
36. E. Blöchliger, M. Blocher, P. Walde, P. L. Luisi, *J. Phys. Chem. B* **102**, 10383 (1998).
37. We thank A. Keefe, P. L. Luisi, B. Seelig, P.-A. Monnard, I. Chen, K. Ashtiani-Salehi, and A. Luptak for their helpful comments on the manuscript and P. L. Luisi for helpful discussions and communication of results before publication. This work was supported by grants from the Human Frontier Science Program and the NASA Astrobiology Institute. M.M.H. was supported by an NIH National Research Service Award. S.M.F. was supported by a National Science Foundation Graduate Research Fellowship. J.W.S. is an Investigator of the Howard Hughes Medical Institute.

Supporting Online Material
www.sciencemag.org/cgi/content/full/302/5645/618/DC1
Materials and Methods
Figs. S1 to S4
References

31 July 2003; accepted 24 September 2003

Glacial Earthquakes

Göran Ekström,[1]* Meredith Nettles,[1] Geoffrey A. Abers[2]

We have detected dozens of previously unknown, moderate earthquakes beneath large glaciers. The seismic radiation from these earthquakes is depleted at high frequencies, explaining their nondetection by traditional methods. Inverse modeling of the long-period seismic waveforms from the best-recorded earthquake, in southern Alaska, shows that the seismic source is well represented by stick-slip, downhill sliding of a glacial ice mass. The duration of sliding in the Alaska earthquake is 30 to 60 seconds, about 15 to 30 times longer than for a regular tectonic earthquake of similar magnitude.

Most earthquakes follow a simple scaling relationship such that the duration of fault movement is proportional to $10^{M/2}$, where M is the earthquake moment magnitude. The typical duration of an $M = 5$ earthquake is 2 s, and an $M = 7$ earthquake, 20 s. The short duration of seismic energy release leads to efficient radiation of high-frequency ($f \sim 1$ Hz) seismic waves, and first-arriving, high-frequency P waves are traditionally used to detect and locate seismic events. Earthquakes with durations much longer than normal radiate less energy at the frequencies used for earthquake monitoring and may go undetected.

Earthquakes with durations of thousands of seconds cannot be detected by seismometers because they do not generate elastic waves. Such earthquakes have, however, been detected geodetically (*1*–*5*). Very-long-period (1 to 10 mHz) seismic data have been used in attempts to detect and locate moderate and large ($M \geq 5.0$) earthquakes with durations of tens to hundreds of seconds, with ambiguous results (*6*–*8*).

Here, we use a recently developed method (*9*) to detect and locate sources of long-period seismic surface waves on a global scale. The detection and location algorithm has its basis in standard array-processing techniques. Vertical-component seismograms from about 100 seismometers around the world are filtered between 35- and 150-s period and phase adjusted to correct for Rayleigh wave propagation delays from a given test location to each station. Any Rayleigh wave signal emanating from the test location will then be in phase across the stations of the global array, and the signals can be analyzed for the simultaneous presence of coherent energy (fig. S1). Continuous seismic data are analyzed for detections on a dense grid of test locations covering the surface of the Earth (*10*).

Application of the algorithm to 3 years of data, 1999 to 2001, has led to the detection and location of 7292 events. The smallest earthquake detected has an estimated magnitude (*11*) of $M = 4.6$. All but 521 of the events are correlated spatially and temporally with earthquakes already reported in various global bulletins of seismicity. Of the 521 previously unknown events, about 450 occur along plate boundaries or in other tectonically active zones. Many are located along the ridge-transform system in the Southern

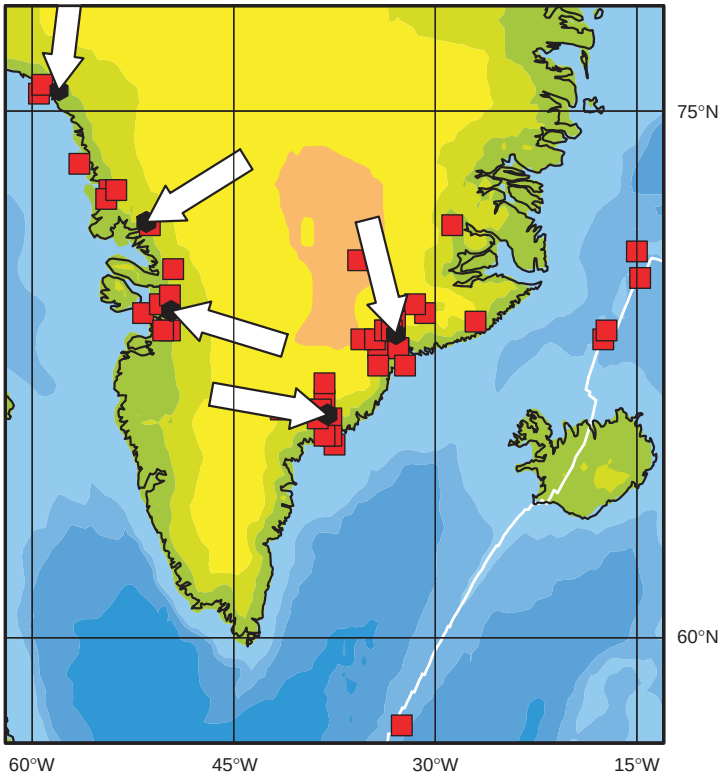

Fig. 1. Topographic map of southern Greenland and vicinity. The white line shows the location of the northern mid-Atlantic ridge. Red squares show the locations of detected earthquakes not previously reported in the earthquake bulletins of the NEIC or the ISC. Five previously unknown earthquakes were detected in the seismically active region near the plate boundary, and 42 previously unknown earthquakes ($4.6 \leq M \leq 5.0$) were detected near the coast of Greenland. White arrows show the horizontal slip azimuths obtained in CSF inversions of teleseismic data for five well-recorded events (on 19 April 1999, 24 April 1999, 16 August 2000, 15 September 2000, and 28 December 2001; see table S1). The black hexagon at the tip of each arrow indicates the centroid location obtained in the inversion.

[1]Department of Earth and Planetary Sciences, Harvard University, 20 Oxford Street, Cambridge, MA 02138, USA. [2]Department of Earth Sciences, Boston University, 685 Commonwealth Avenue, Boston, MA 02215, USA.

*To whom correspondence should be addressed. E-mail: ekstrom@seismology.harvard.edu

Hemisphere, where it is known that traditional detection methods occasionally fail to detect regular $M \sim 5$ earthquakes (*7*, *12*).

Of the remaining earthquakes, 46 are located in glaciated areas. Forty-two of the earthquakes of $4.6 \leq M \leq 5.0$ are located beneath Greenland (Fig. 1, table S1), an area otherwise known for its low level of seismicity (*13*). One earthquake is located in the Denali range, Alaska (Fig. 2), and three earthquakes are located on the Antarctic coast.

The Alaska earthquake ($M = 5.0$) occurred within the regional Alaska Seismographic Network, which in this area normally detects and reports earthquakes of much smaller magnitudes, often below $M = 1.0$. In addition to being recorded well at globally distributed stations at teleseismic distances, the earthquake was serendipitously recorded by instruments of the BEAAR (Broadband Experiment Across the Alaska Range) experiment (*14*), a temporary deployment of PASSCAL (Program for Array Seismic Studies of the Continental Lithosphere) broadband seismometers. These data provided an opportunity to investigate the source characteristics of one of the previously undetected glacial earthquakes in greater detail.

Short-period seismograms for the Alaska earthquake recorded at the BEAAR array have unusually small amplitudes. At a distance of 200 km from the epicenter, the maximum short-period amplitude is only 5% of that of a regular $M = 4.2$ earthquake (Fig. 3). Long-period seismograms for the glacial event have large amplitudes and show a complex, low-frequency surface-wave arrival, indicating a source-process time of tens of seconds.

The long-period data from the BEAAR array were used together with long-period surface waves from the global network to model the seismic source. We initially used the Harvard centroid-moment-tensor (CMT) method (*15*, *16*) to invert for a standard moment-tensor source. These inversions failed to fit the phase of the Rayleigh and Love waves for the nine closest-in stations and did not result in a stable centroid location. We concluded that a moment tensor, the standard physical model for earthquake sources, was inadequate to represent the forces active in this earthquake.

Our inability to model the waveforms satisfactorily with a standard, faulting source model, together with the direct association of the new earthquakes with major glaciers, led us to consider alternative models. The long-period seismic signals from large landslides have been successfully modeled with single forces (*17*, *18*). When a slide initiates, the ground beneath the sliding mass rebounds elastically up-dip as the sliding mass gains momentum in the opposite direction. At the end of the sliding episode, the sliding mass loses momentum, and a frictional force is again applied to the underlying ground in the down-dip sliding direction. We formalize the inversion for this class of sources following Kawakatsu (*18*) and parameterize our inversion in terms of a centroid single force (CSF).

The CSF inversion leads to a stable result and a better fit of the synthetic seismograms to the data than that achieved with the CMT inversion (*19*). In particular, the phase of the Rayleigh and Love waves is well predicted by the CSF source. At a few stations located nearly perpendicular to the sliding direction, the nearly nodal Rayleigh waves have a minor phase shift with respect to the model predictions. This may be caused by a number of factors, including a spatially extended source, a small change in sliding direction during the event, or refraction of the Rayleigh wave as it travels along the Denali range and the deeper, subducted slab.

The CSF analysis results in an improved estimate of the location of the long-period source and the geometry and magnitude of the active forces. The seismograms provide good constraints on a location at 62.66°N and 152.43°W. This location agrees with an estimate obtained from polarization analysis of Rayleigh waves and with short-period *P*-wave arrival times at the four closest stations. We estimate the uncertainty in the CSF location to be 15 to 30 km. The seismic location is only ~15 km west of the Dall glacier, and we therefore believe that the earthquake is likely to be associated with this glacier. The geometry of the CSF corresponds to a sliding azimuth of

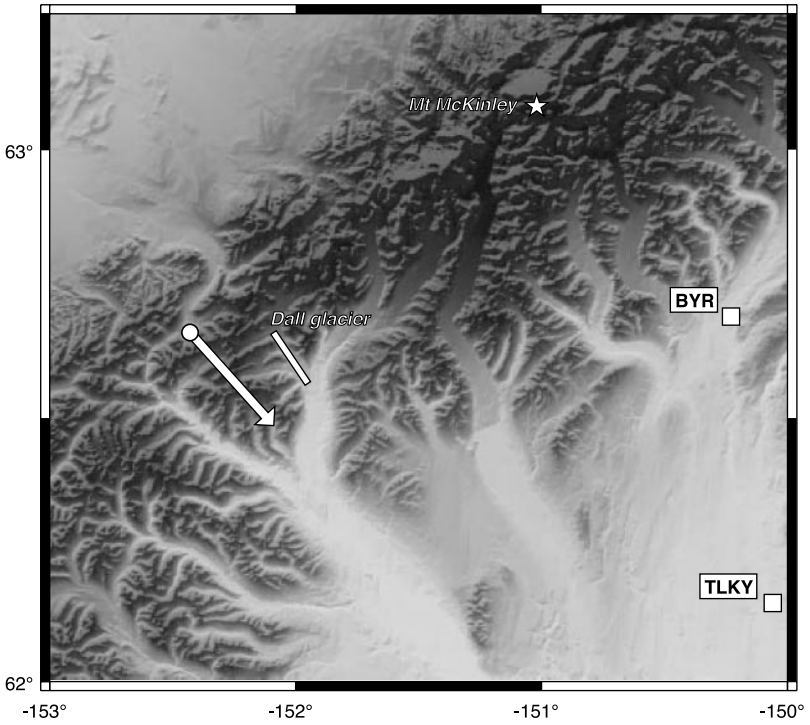

Fig. 2. Topographic map of the epicentral area of the Alaska earthquake, showing the locations of the two BEAAR stations closest to the earthquake (squares) and the earthquake location (circle) and horizontal direction of sliding (arrow) determined in the CSF inversion. Note the similarity between the geometry of the Dall glacier (shown by the white bar) and the sliding azimuth.

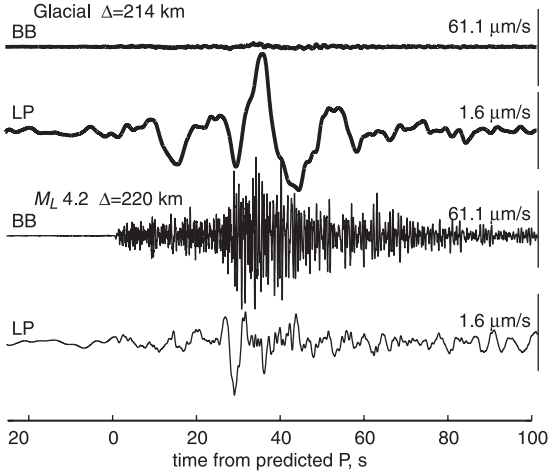

Fig. 3. Seismograms from the Alaska glacial event (4 September 1999, 15:15:20.0) (top two traces) and a nearby, tectonic, $M = 4.2$ earthquake (bottom two traces) recorded at comparable distances (Δ) by BEAAR stations YAN and GOO. For each trace pair, top shows broadband (BB) (0.00833 to 20 Hz) velocity record, and bottom shows filtered long-period (LP) (0.01 to 0.2 Hz) velocity record. Vertical scale is shown by labeled height of line on right. The seismograms are aligned at the predicted *P*-wave arrival time.

138°, consistent with the down-slope direction of the Dall glacial valley (Fig. 2). The down-dip slope of the sliding motion is 9°, somewhat steeper than the glacial valley. This quantity is less well constrained than the azimuth, and a horizontal CSF fits the data nearly as well.

The CSF analysis yields an estimate of the twice-time-integrated active force couple, which in the mass-sliding model can be interpreted as the product of mass and distance (*18*). For the Dall glacier event, the value of this parameter is 1.3×10^{14} kg m, corresponding to, for example, the displacement of 10 km^3 of ice by 13 m. We are, however, not able to place independent constraints on mass or distance, so movements of larger or smaller masses over shorter or longer distances are equally consistent with our results. The difference between the earthquake origin time determined from the short-period seismograms and the centroid time is 26 s. Examination of the local long-period seismograms and visual comparison with synthetic waveforms generated for different source durations indicate that the earthquake duration was longer than 30 s and shorter than 60 s. We used a source-process time of 40 s in the inverse modeling of the waveforms. The derived source parameters are not sensitive to the duration within the range 30 to 60 s.

Examination of several of the newly detected earthquakes beneath Greenland (Fig. 1) indicates that they are analogous to the Dall glacier earthquake, and we infer that they are examples of a previously unknown class of earthquake associated with rapid mass movement in glaciers. We speculate that the dynamics of the seismic events are controlled by stick-slip motion of the glacier along its basal surface and that the phenomenon involves the displacement of a large mass over a relatively short distance. Microearthquakes occur in association with glaciers (*20*, *21*), and some have been linked to sliding motion on so-called sticky spots (*22*–*24*), which represent patches of resistance to slip along the glacier base. Rapid variations in pore pressure at the glacier base (*25*) or the nonlinear weakening of a deforming till (*26*) may generate conditions for rapid lowering of the effective friction, growth of a slipping patch, and sudden large-scale motion of the glacier. Whether the newly detected earthquakes belong to a distribution of glacial slip events with well-defined size-duration and size-frequency relationships remains an open question.

A seasonal variation in the frequency of glacial earthquakes on Greenland is seen in the data (table S1), with fewer events occurring from January to March than during the rest of the year. The small number of earthquakes detected on Antarctica as compared with Greenland also suggests that climate influences the conditions necessary to cause or trigger glacial earthquakes. Surface melting, which is widespread in Greenland during the summer (*27*), is likely to cause increased water pressure at the base of the glacier (*28*) and may be one important trigger for the earthquakes. Additional investigations, such as by continuous Global Positioning System monitoring and close-in broadband seismic recording, are needed to elucidate further the physical processes responsible for these glacial earthquakes.

References and Notes

1. H. Dragert, K. Wang, T. S. James, *Science* **292**, 1525 (2001).
2. M. M. Miller, T. Melbourne, D. J. Johnson, W. Q. Sumner, *Science* **295**, 2423 (2002).
3. A. T. Linde, M. T. Gladwin, M. J. S. Johnston, R. L. Gwyther, R. G. Bilham, *Nature* **383**, 65 (1996).
4. K. Heki, S. Miyazaki, H. Tsuji, *Nature* **386**, 595 (1997).
5. S. Miyazaki, J. J. McGuire, P. Segall, *J. Geophys. Res.* **108**, 2087 (2003).
6. G. C. Beroza, T. H. Jordan, *J. Geophys. Res.* **95**, 2485 (1990).
7. P. M. Shearer, *J. Geophys. Res.* **99**, 13713 (1994).
8. G. Ekström, *J. Geophys. Res.* **106**, 26483 (2001).
9. G. Ekström, M. Nettles, *Eos* **83**, F1037 (2002).
10. Materials and Methods are available as supporting material on *Science* Online.
11. The magnitude is calculated from the amplitudes of teleseismic Rayleigh waves with a dominant period of 50 s. The scale has been calibrated against the moment magnitudes (M_w) of shallow earthquakes in the Harvard CMT catalog (*15*).
12. D. Rouland, C. Condis, C. Parmentier, A. Souriau, *Bull. Seismol. Soc. Am.* **82**, 2448 (1992).
13. The National Earthquake Information Center (NEIC) of the U.S. Geological Survey (USGS) and the International Seismological Centre (ISC) located three earthquakes beneath Greenland from 1999 to 2001 with magnitudes of 4.7, 3.6, and 3.2. None of these are within 300 km of the events reported here.
14. G. A. Abers *et al.*, *Seismol. Res. Lett.* **73**, 219 (2002).
15. A. M. Dziewonski, T.-A. Chou, J. H. Woodhouse, *J. Geophys. Res.* **86**, 2825 (1981).
16. R. Arvidsson, G. Ekström, *Bull. Seismol. Soc. Am.* **88**, 1003 (1998).
17. H. Kanamori, J. W. Given, *J. Geophys. Res.* **87**, 5422 (1982).
18. H. Kawakatsu, *J. Geophys. Res.* **94**, 12363 (1989).
19. Long-period Love and Rayleigh waves recorded at 89 stations of the BEAAR array and the Global Seismographic Network (GSN) were fit in the inversions. The variance reduction for the CMT inversion was 29%; for the CSF inversion, 44%.
20. D. VanWormer, E. Berg, *J. Glaciol.* **12**, 259 (1973).
21. L. W. Wolf, J. N. Daview, *Bull. Seismol. Soc. Am.* **76**, 367 (1986).
22. D. D. Blankenship, S. Anandakrishnan, J. L. Kempf, C. F. Bentley, *Ann. Glaciol.* **9**, 30 (1987).
23. R. B. Alley, *J. Glaciol.* **39**, 447 (1993).
24. S. Anandakrishnan, C. R. Bentley, *J. Glaciol.* **39**, 455 (1993).
25. B. Kamb *et al.*, *Science* **277**, 469 (1985).
26. B. Kamb, *J. Geophys. Res.* **96**, 16585 (1991).
27. E. Rignot, R. H. Thomas, *Science* **297**, 1502 (2002).
28. H. J. Zwally *et al.*, *Science* **297**, 218 (2002).

29. Supported by NSF grants EAR-0207608 (G.E.) and EAR-9996451 (G.A.A.) and an NSF Graduate Fellowship (M.N.). The GSN data were collected and distributed by the Incorporated Research Institutes for Seismology (IRIS) and the USGS.

Supporting Online Material

www.sciencemag.org/cgi/content/full/1088057/DC1
Materials and Methods
Fig. S1
Table S1

16 June 2003; accepted 9 September 2003
Published online 25 September 2003;
10.1126/science.1088057
Include this information when citing this paper.

Air Pollution and Climate-Forcing Impacts of a Global Hydrogen Economy

Martin G. Schultz,[1]* Thomas Diehl,[1] Guy P. Brasseur,[1] Werner Zittel[2]

If today's surface traffic fleet were powered entirely by hydrogen fuel cell technology, anthropogenic emissions of the ozone precursors nitrogen oxide (NO_x) and carbon monoxide could be reduced by up to 50%, leading to significant improvements in air quality throughout the Northern Hemisphere. Model simulations of such a scenario predict a decrease in global OH and an increased lifetime of methane, caused primarily by the reduction of the NO_x emissions. The sign of the change in climate forcing caused by carbon dioxide and methane depends on the technology used to generate the molecular hydrogen. A possible rise in atmospheric hydrogen concentrations is unlikely to cause significant perturbations of the climate system.

It is now widely accepted that the increased combustion of fossil fuels since the industrialization of the Western world has led to unprecedented changes in the chemical composition of Earth's atmosphere, with multiple consequences for regional air quality and the global climate system (*1*, *2*). For example, despite efforts in several countries to control emissions from car exhaust and stationary sources, the hemispheric background concentrations of tropospheric ozone did not decline after 1985, when catalytic converters were introduced in the United States and Europe (*3*, *4*). On the contrary, many regions in the world have observed a serious degradation of air quality over the past decade, due to increased motorized traffic and industrial emissions (*5*).

[1]Max-Planck-Institut für Meteorologie, Bundesstraße 55, 20146 Hamburg, Germany. [2]Ludwig-Bölkow-Systemtechnik, Daimlerstraße 15, 85521 Ottobrunn, Germany.

*To whom correspondence should be addressed. E-mail: martin.schultz@dkrz.de